THE JOURNAL OF BIOLOGICAL CHEMISTRY VOL. 287, NO. 50, pp. 41851–41860, December 7, 2012

Subunit-specific Incorporation Efficiency and Kinetics in Mitochondrial Complex I Homeostasis*

Received for publication, June 19, 2012, and in revised form, October 1, 2012 Published, JBC Papers in Press, October 4, 2012, DOI 10.1074/jbc.M112.391151

Cindy E. J. Dieteren[‡§¶], Werner J. H. Koopman[‡], Herman G. Swarts[‡], Janny G. P. Peters[‖], Piotr Maczuga[§], Jasper J. van Gemst[§], Rosalinde Masereeuw[‖], Jan A. M. Smeitink[§], Leo G. J. Nijtmans[§], and Peter H. G. M. Willems[‡1]

From the Departments of [‡]Biochemistry, [§]Pediatrics, [¶]Cell Biology, and [‖]Pharmacology and Toxicology, Nijmegen Centre for Molecular Life Sciences, Radboud University Nijmegen Medical Centre, 6500 HB Nijmegen, The Netherlands

Background: The dynamics of subunit incorporation in complex I (CI) under steady-state conditions are still elusive.
Results: GFP-labeled CI subunits replace their endogenous counterparts in CI with different efficiencies and rates within 24 h of induction.
Conclusion: CI maintenance involves continuous subunit replacement by direct exchange or through assembly intermediates.
Significance: Elucidating subunit replacement in CI is vital as subunits are continuously threatened by oxidative damage.

Studies employing native PAGE suggest that most nDNA-encoded CI subunits form subassemblies before assembling into holo-CI. In addition, *in vitro* evidence suggests that some subunits can directly exchange in holo-CI. Presently, data on the kinetics of these two incorporation modes for individual CI subunits during CI maintenance are sparse. Here, we used inducible HEK293 cell lines stably expressing AcGFP1-tagged CI subunits and quantified the amount of tagged subunit in mitoplasts and holo-CI by non-native and native PAGE, respectively, to determine their CI incorporation efficiency. Analysis of time courses of induction revealed three subunit-specific patterns. A first pattern, represented by NDUFS1, showed overlapping time courses, indicating that imported subunits predominantly incorporate into holo-CI. A second pattern, represented by NDUFV1, consisted of parallel time courses, which were, however, not quantitatively overlapping, suggesting that imported subunits incorporate at similar rates into holo-CI and CI assembly intermediates. The third pattern, represented by NDUFS3 and NDUFA2, revealed a delayed incorporation into holo-CI, suggesting their prior appearance in CI assembly intermediates and/or as free monomers. Our analysis showed the same maximum incorporation into holo-CI for NDUFV1, NDUFV2, NDUFS1, NDUFS3, NDUFS4, NDUFA2, and NDUFA12 with nearly complete loss of endogenous subunit at 24 h of induction, indicative of an equimolar stoichiometry and unexpectedly rapid turnover. In conclusion, the results presented demonstrate that newly formed nDNA-encoded CI subunits rapidly incorporate into holo-CI in a subunit-specific manner.

Mitochondrial NADH:ubiquinone oxidoreductase or complex I (CI;[2] EC 1.6.5.3) is the largest enzyme of the oxidative phosphorylation system. It catalyzes the oxidation of NADH and reduction of ubiquinone, utilizing the energy generated by this process to translocate protons across the mitochondrial inner membrane (1). Human CI consists of at least 44 different subunits (2), with seven encoded by the mitochondrial DNA (mtDNA) and the remainder by the nDNA. The manner in which this intricate enzyme is maintained is only beginning to be understood.

According to the current view on CI assembly, subunits of the dehydrogenase, hydrogenase, and proton-translocation module assemble via several intermediates into the L-shaped holoenzyme (3–9). In addition to the *de novo* CI assembly pathway, a CI subunit exchange pathway was proposed, in which specific subunits (NDUFV1, NDUFV2, NDUFV3, NDUFS6, and NDUFS4) directly replace their preexisting counterparts in holo-CI, whereas other subunits (NDUFB8, NDUFS1, NDUFS2, NDUFS7, NDUFS8, NDUFA9, NDUFA10) lack this capability (8) (see Table 1 for subunit nomenclature in different species). However, the extent to which these two incorporation manners are applied under physiological conditions remains to be elucidated.

Although a basic framework for human CI assembly has been established, the turnover and assembly dynamics of individual CI subunits under non-disturbed, steady-state conditions remain largely unknown. Pulse labeling studies in the fungus *Neurospora crassa* revealed that newly synthesized subunits assemble at different rates into holo-CI (10). This suggests that not all CI subunits are imported, assembled, exchanged, and/or maintained at similar rates. Only few studies have investigated the assembly dynamics of mammalian CI (3, 8, 11–14). Pulse labeling studies established that, in general, nDNA-encoded subunits appear faster in holo-CI than mtDNA-encoded subunits (8, 11). After complete depletion of CI by transient inhibition of mitochondrial translation, osteosarcoma cells needed 2–4 days to normalize their CI level (3, 12, 14). A similar restoration time was observed after inducible HA-tagged NDUFA1 expression in NDUFA1-deficient Chinese hamster cells (13). In

* This work was supported by the Netherlands Organization for Scientific Research (Grant 911-02-008) and a grant from the Radboud University Nijmegen Medical Centre (to W. J. H. K. and L. G. J. N).
[1] To whom correspondence should be addressed: Biochemistry (286), Nijmegen Centre for Molecular Life Sciences, Radboud University Nijmegen Medical Centre, P.O. Box 9101, NL-6500 HB Nijmegen, The Netherlands. Tel.: 31-24-3614589; Fax: 31-24-3616413; E-mail: p.willems@ncmls.ru.nl.
[2] The abbreviations used are: CI, complex I; AcGFP1, *Aequorea coerulescens* GFP; BN-PAGE, blue native polyacrylamide gel electrophoresis; MW, molecular weight; NDUF, NADH dehydrogenase ubiquinone flavoprotein; IGA, in-gel activity; EGFP, enhanced GFP.

TABLE 1

Nomenclature of CI subunits investigated in this study

Core subunits are shown in boldface type. n.p., not present; Hs, *Homo sapiens*; Bt, *Bos taurus*; Yl, *Yarrowia lipolytica*; Tt, *Thermus thermophilus*; Ec, *Escherichia coli*.

Hs	Bt	Yl	Tt	Ec
NDUFV1	**51-kDa**	**NUBM**	**Nqo1**	**NuoF**
NDUFV2	**24-kDa**	**NUHM**	**Nqo2**	**NuoE**
NDUFS1	**75-kDa**	**NUAM**	**Nqo3**	**NuoG**
NDUFS2	**49-kDa**	**NUCM**	**Nqo4**	**NuoCD**
NDUFS3	**30-kDa**	**NUGM**	**Nqo5**	**NuoCD**
NDUFS7	**PSST**	**NUKM**	**Nqo6**	**NuoB**
NDUFS8	**TYKY**	**NUIM**	**Nqo9**	**NuoI**
NDUFS4	AQDQ	NUYM	n.p.	n.p.
NDUFS6	13 kDa	NUMM	n.p.	n.p.
NDUFA2	B8	NI8M	n.p.	n.p.
NDUFA12	B17.2	N7BM	n.p.	n.p.
NDUFA1	MWFE	NIMM	n.p.	n.p.
NDUFB6	B17	n.p.	n.p.	n.p.
NDUFB8	ASHI	NIAM	n.p.	n.p.

these mutant Chinese hamster fibroblasts, holo-CI formation clearly lagged behind the increase in NDUFA1-HA, suggesting that this subunit first appears in a precomplex, without using an exchange route in parallel (13). However, the dynamics of subunit incorporation during these CI depletion/restoration experiments are very likely to differ from the natural assembly kinetics during undisturbed CI maintenance because (i) direct subunit exchange in non-existing CI is per definition not possible and (ii) the pool sizes of individual subunits and subassemblies alter upon CI depletion (3, 4, 13, 15–19).

There are still many aspects of mammalian CI homeostasis that remain to be elucidated. For instance, no definite data are available on (i) the incorporation efficiency of imported CI subunits into holo-CI, (ii) the stoichiometry of CI subunits in holo-CI, and (iii) the incorporation kinetics of individual CI subunits. In this study, we addressed these topics using inducible human embryonic kidney (HEK293) cells for tunable expression of AcGFP1-tagged CI subunits (4, 18–21). Evidence is provided that CI subunits use subunit-specific pathways to assemble into holo-CI and that at least seven of these are present in an equimolar stoichiometry in the holocomplex.

EXPERIMENTAL PROCEDURES

Generation and Culturing of Inducible Cell Lines—Gateway™ Entry vectors (Invitrogen) containing CI subunit open reading frames without stop codon (NDUFV1, NM_007103; NDUFS1, NM_005006; NDUFS2, NM_ 004550; NDUFS3, NM_004551; NDUFS7, BC 111517; NDUFS8, NM_002496; NDUFS4, NM_002495; NDUFS6, BC_046155; NDUFA2, NM_002488; NDUFA12, NM_018838; NDUFA1, NM_ 004541; NDUFB6, NM_002493; transcript variant 1) or the COX8 mitochondrial targeting sequence (first 210 base pairs of sequence NM_00004074) were created as described previously (19). Entry clones containing NDUFV2 (BC_001632; clone HsCD0000415552), NDUFB8 (BC_000466; clone HsCD00042304) without stop codon were ordered from The Plasmid Database (22). A destination vector containing the AcGFP1 sequence (Clontech, Westburg, Leusden, The Netherlands) in-frame behind Gateway Reading Frame Cassette B (Invitrogen) and a Flp Recombination Target site for targeted genomic integration in Flp-in T-Rex293 cells was created as described previously (19). Expression clones were generated by recombining the entry clones with the destination vector by using Gateway LR Clonase II enzyme mix (Invitrogen) (for details, see Ref. 19). Expression vectors were co-transfected with the pOG44 vector (Invitrogen) in Flp-in T-Rex293 cells (Invitrogen) using Superfect transfection Reagent (Qiagen, Venlo, The Netherlands). Cells were cultured for selection in DMEM (Biowhitaker, Walkersville, MD) supplemented with 10% (v/v) fetal calf serum (FCS) (PAA Laboratories, Pasching, Austria), 1% penicillin/streptomycin (Invitrogen), 200 μg/ml hygromycine (Calbiochem, Brunschwig, Amsterdam, The Netherlands), and 50 μg/ml blasticin (Invitrogen). For induction of overexpression, doxycycline was added at a concentration of 1 μg/ml for 24 h.

Quantitative Real-time PCR—RNA was isolated from cell pellets from two independent cultures using TRIzol reagent (Invitrogen) according to the manufacturer's instructions. RNA was dissolved in RNase-free water at 65 °C and diluted to a final concentration of 200 ng/μl. Reverse transcription was performed in a total mixture of 40 μl containing 2 μg of RNA, 1× first strand buffer (Invitrogen), 0.01 M DTT (Invitrogen), 1 mM dNTP mix, 200 units of Superscript II reverse transcriptase (Invitrogen), 60 units of RNAsin (Promega, Madison, WI), 625 ng oligo(dT) primers (Promega), and 125 pmol of random primers (Promega). This reaction mixture was incubated at 42 °C for 1 h and at 96 °C for 3 min. The cDNA samples of two independent experiments were analyzed on two different days by quantitative real-time PCR. Separate real-time PCR reactions were performed for AcGFP1, β-actin, and 18 S ribosomal RNA (18 S rRNA) on 50 ng of cDNA using SybrGreen PCR Master Mix (Applied Biosystems, Zwijndrecht, The Netherlands), 15 pmol of forward primer and 15 pmol of reverse primer in a reaction volume of 25 μl. Primers were designed by PrimerExpress Software (Applied Biosystems). The primer pairs used were as follows: AcGFP1_fwd 5′-gaggatgacggcaactacaagtc-3′ with AcGFP1_rev, 5′-acacattgtgggcgttgtagtt-3′; β-actin_fwd, 5′-cgtggacatccgcaaagac-3′ with β-actin_rev, 5′-ctcaggaggagcaatgatcttgat 3′; 18 S rRNA_fwd, 5′-GTAACCCGTTGAACCCCATT-3′ with 18 S rRNA_rev, 5′-CCATCCAATCGGTAGTAGCG-3′. Thermal cycling conditions were set as follows: 2 min at 50 °C and 10 min at 95 °C, followed by 40 cycles of 15 s at 95 °C and 1 min at 60 °C. Amplification of a single product for each primer set was first confirmed by electrophoresis on a 2% agarose gel. PCR amplification and detection was performed using an ABI Prism 7900 HT Sequence Detection System (Applied Biosystems). A comparative threshold cycle (C_T) method was used to quantify the gene expression of AcGFP1-tagged CI subunits in different cell lines. As a calibrator, we analyzed AcGFP1-expression in a cell line expressing matrix-targeted AcGFP1 (named GFP). To compare the expression in different cell lines, the C_T of β-actin was subtracted from the C_T of GFP to yield the ΔC_T. The expression of AcGFP1-tagged CI subunits was expressed as $2^{-\Delta\Delta C_T}$, where $\Delta\Delta C_T = (\Delta C_T \text{GFP}) - (\Delta C_T \text{ AcGFP1-tagged CI subunit})$. Normalization to 18 S rRNA was performed in a similar way to confirm results obtained using β-actin. Statistical analysis was performed using Origin Pro (version 7.5, Originlabs, Northampton, MA). Values are expressed as mean ± S.D.

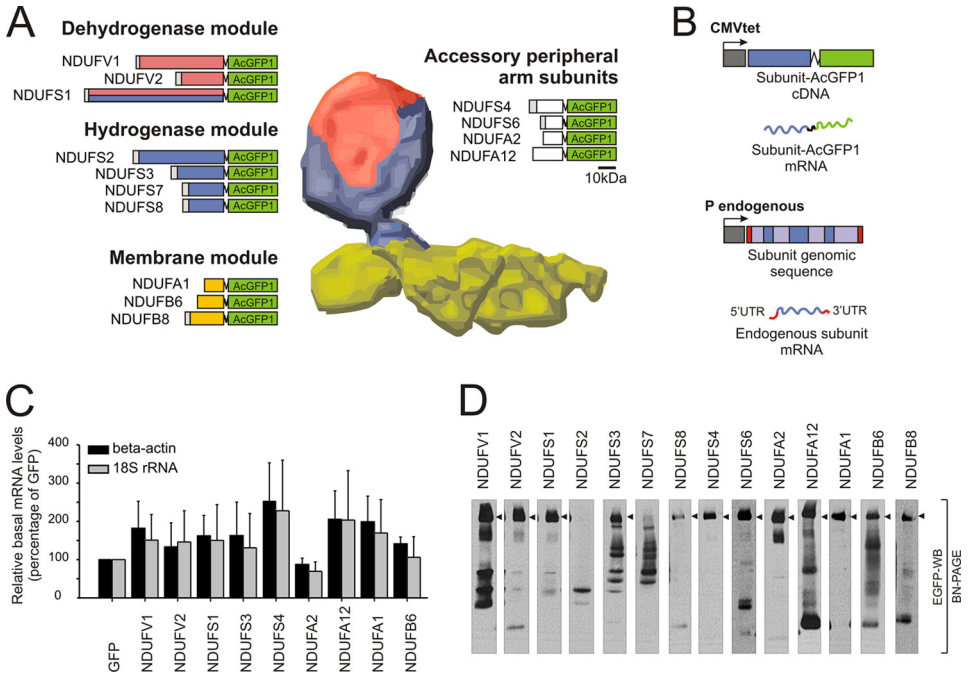

FIGURE 1. **Characterization of inducible cell lines expressing AcGFP1-tagged CI subunits.** *A*, schematic representation of holo-CI depicting the dehydrogenase (*red*), hydrogenase (*blue*), and proton-translocation module (*yellow*), and subunits that were selected for investigation. Four subunits (*white*), yet without any module-classification, were included. The open reading frames of these subunits were fused to the AcGFP1 sequence by a linker and cloned behind a tetracycline-inducible promoter. N-terminal mitochondrial targeting sequences are depicted in *gray*. The relative size of the constructs is shown by length of the coding region (*scale bar*, 10 kB). *B*, Flp-in T-Rex293 cells integrate constructs into a single target site in their genome. The resulting transcripts do not contain their original 3′- and 5′-untranslated region (UTR) sequences that often have mRNA-stabilizing and/or translation efficiency regulating elements. *CMVtet*, tetracycline-inducible promoter; *P endogenous*, endogenous promoter. *C*, transcript levels of AcGFP1-tagged CI subunits and matrix-targeted AcGFP1 as determined by quantitative real-time PCR. Cell lines were cultured in normal growth medium, resulting in low steady-state expression (leakage). Data were related to the value obtained with matrix-targeted AcGFP1 (referred to as GFP) after normalization to β-actin or 18 S rRNA. The values presented are the mean ± S.D. *D*, assembly profiles of AcGFP1-tagged subunits. Mitoplasts of cells cultured in normal growth medium were subjected to BN-PAGE followed by Western blotting (*WB*) and immunodetection with anti-EGFP antibody. The height of holo-CI is indicated with *filled arrowheads*. Exposure times of blots are adjusted for optimal visualization.

BN-PAGE and SDS-PAGE Analysis—Mitoplasts were isolated from cell pellets using digitonin, and mitochondrial protein complexes were solubilized using *n*-dodecyl β-D-maltoside as described previously (23). BN-PAGE 5–15% gradient gels were loaded with 40–80 μg protein and scanned for fluorescence (473 excitation laser, FITC filter >510 nm) using a FLA5000 fluorescence image analyzer (Fujifilm, Tilburg, The Netherlands). Subsequently, CI in-gel activity (IGA) assays were performed, or proteins were blotted to a nitrocellulose membrane. A small fraction of the mitochondrial lysates was denatured and loaded on 10% SDS-PAGE gels as described previously (4), scanned for fluorescence and blotted to nitrocellulose. Immunodetection was performed using primary antibodies raised against EGFP (a gift from Dr. F. J. van Kuppeveld, Nijmegen, the Netherlands), succinate dehydrogenase complex subunit A (Invitrogen), NDUFV2 (Sigma, Zwijndrecht, The Netherlands), NDUFS2 (a gift from Prof. B. Robinson, Toronto, Canada), NDUFS3 (Invitrogen), NDUFS4 (Mitosciences, Eugene, OR), NDUFA2 (4), NDUFA1 (a gift from Prof. I. Scheffler, San Diego, CA), and NDUFB6 (Invitrogen). Secondary antibodies were peroxidase-conjugated anti-mouse or anti-rabbit IgGs (Invitrogen). Chemoluminescence (Pierce, Thermo Fisher Scientific, Etten-Leur, The Netherlands) was detected on film or on a LAS-3000 luminescent image analyzer (Fujifilm).

Image Processing and Quantification—Integrated optical density of signals obtained by fluorescence scanning, immunodetection, and IGA assays were quantified using Image Pro Plus 5.1 (Media Cybernetics, Bethesda, MD). As a measure for total amount of AcGFP1-tagged CI subunits in mitoplasts, the integrated optical density of AcGFP1-specific bands of the expected molecular weight was determined after SDS-PAGE and expressed relative to the IGA-signal after BN-PAGE (to correct for loading differences between samples). The relative amount of AcGFP1-tagged subunits incorporated into holo-CI was calculated from AcGFP1-specific bands at the height of CI after BN-PAGE and corrected for the IGA-signal (to correct for loading differences between samples).

RESULTS

Incorporation of AcGFP1-tagged CI Subunits into Holo-CI—To study the incorporation kinetics of nDNA-encoded subunits into holo-CI, we used a panel of Flp-In T-Rex293 cell lines engineered to express AcGFP1-tagged versions of these subunits in a doxycycline-inducible manner (4, 19, 20). In the remainder of the paper, the prefix "t" is used to indicate the tagged version of the subunit in question. Apart from the seven nDNA-encoded core subunits (NDUFV1, NDUFV2, NDUFS1, NDUFS2, NDUFS3, NDUFS7, and NDUFS8) we also investigated seven accessory subunits (NDUFS4, NDUFS6, NDUFA1, NDUFA2, NDUFA12, NDUFB6, and NDUFB8), predicted to constitute part of either the peripheral or membrane arm of CI (Fig. 1*A*).

In theory, the cellular transcript levels of the tagged CI subunits should be the same because we used targeted recombination, meaning that cDNAs were integrated at the same position in the genomic DNA and lacked the 5′ and 3′ post-transcriptional regulatory elements (Fig. 1*B*). Indeed, quantitative RT-PCR analysis revealed no significant difference in the amount of transcripts between the various cell lines (Fig. 1*C*). BN-PAGE of mitoplast fractions followed by Western blotting with an anti-GFP antibody showed that all cell lines expressed the AcGFP1-tagged subunit (Fig. 1*D*). Optimal exposure of each individual lane revealed that the tagged CI subunits were generally incorporated in holo-CI (*filled arrowhead*) and in some cases also in lower MW subcomplexes. Exceptions were tNDUFS2 and tNDUFS7, which were clearly detectable in lower MW subcomplexes but hardly in holo-CI.

Mitoplast Accumulation and Holo-CI Incorporation of AcGFP1-tagged CI Subunits at a High Level of Induction—Expression of tagged subunits was increased by culturing the cells in the presence of 1 μg/ml doxycycline for 24 h. Next, we isolated mitoplasts, separated their constituent proteins by SDS-PAGE, and determined the total amount of tagged subunit. Fluorescence scanning of the obtained gels demonstrated the presence of both intact tagged subunit (*filled arrowheads*) and breakdown products with a lower MW (Fig. 2*A*). To assess the amount of tagged subunit incorporated into holo-CI, we analyzed the same mitoplast preparations using BN-PAGE. Comparison of the resulting BN-PAGE fluorogram (Fig. 2*B*) with the immunoblot depicted in Fig. 1*D* revealed a similar pattern. Next, the BN-PAGE gel was used for IGA analysis, revealing that all cell lines displayed an IGA-positive band at the height of holo-CI (Fig. 2*C*). The intensity of this band was similar among the various cell lines and not affected by expression induction. This is consistent with our previous studies demonstrating that overexpression of tNDUFV1, tNDUFV2, tNDUFS3, tNDUFA2, tNDUFA12, and tNDUFB6 does not interfere with CI amount and/or activity (4, 19, 20). In Fig. 3 we show additional proof for undisturbed CI activity upon overexpression of the other eight subunits used in this study. Because the cell lines expressing tNDUFS2, tNDUFS7, tNDUFS8, and tNDUFB8 did not to show a detectable fluorescence signal at the height of holo-CI in Fig. 2*B*, they were excluded from further analysis.

To determine the fraction of total mitoplast-tagged subunit present in holo-CI, we quantified the fluorescence intensity at the height of the intact tagged subunit (Fig. 2*A*) and holo-CI (Fig. 2*B*). These intensities were normalized to the corresponding IGA signal (Fig. 2*C*). A similar quantification was performed for a control cell line that expressed AcGFP1 targeted to the mitochondrial matrix ("GFP"). We demonstrated previously that AcGFP1 exclusively localized to mitochondria in this cell line (20). For each gel, the value obtained with GFP was set at 100%, to which all other values were normalized. Fig. 2*D* shows that for a number of cell lines (tNDUFV1, tNDUFS1, tNDUFS4, tNDUFA2, tNDUFS3, tNDUFV2, and tNDUFA12), the amount of tagged subunit present in holo-CI (y axis) was virtually the same (*dotted line*) despite the fact that the total amount of tagged subunit in the mitoplasts (x axis) differed greatly. This suggests that the maximum level of incorporation of tagged subunit into holo-CI was reached and that, most probably, the endogenous subunit was fully replaced by its tagged counterpart. Fig. 2*D* also allows drawing conclusions regarding the efficiency with which an imported tagged subunit is incorporated into holo-CI. A data point on the line of identity (*solid line*) indicates that all tagged subunit in the mitoplasts is part of holo-CI. This condition of maximum incorporation efficiency was observed for tNDUFS1, tNDUFS4, and tNDUFA1.

Evidence That AcGFP1-tagged Subunits Replace Their Endogenous Counterparts in Holo-CI—To substantiate the idea that certain endogenous CI subunits are fully replaced by their tagged counterparts within 24 h of induction, we investigated subunit abundance using specific antibodies (Fig. 4). Mitoplast proteins of cells cultured in the absence (−) and presence (+) of doxycycline were separated by SDS-PAGE. Fluorescence gel scanning confirmed that expression of the tagged subunit increased when doxycycline was present (panels named "fluorescence;" *filled arrowheads*). Subsequent Western blot analysis with anti-subunit antibody was used to reveal the presence of the endogenous subunit (*antibody-WB* panels; *empty arrowheads*). Mitoplasts of cell lines overexpressing tNDUFS3 contained no endogenous subunit, whereas a very weak positive band was obtained with mitoplasts of cells expressing tNDUFA2, tNDUFS4, and tNDUFV2. A clear but markedly reduced band was observed with mitoplasts of cells expressing tNDUFB6. Finally, virtually no change was seen with mitoplasts of cells expressing tNDUFA1 and tNDUFS2, two subunits that were hardly/not incorporated into holo-CI. Noticeably, the anti-NDUFA2 and anti-NDUFS2 antibodies did not recognize the tagged subunits, probably because the tag prevented binding to their epitopes at the C terminus of these subunits. Of note, the observation that for tNDUFS3, tNDUFV2, tNDUFS4, and tNDUFA2 virtually the same fluorescence intensity was measured at the height of holo-CI (Fig. 2*B*) under the condition that nearly all of the endogenous subunit was replaced by its tagged counterpart, provides evidence that the fluorescence intensity values measured for the various subunits are not significantly influenced by differences in fluorescence quantum yield due to differences in location within the complex.

Incorporation Efficiency of AcGFP1-tagged CI Subunits into Holo-CI at a Low Level of Induction—Next, we analyzed the amount of tagged subunit present in mitoplasts (Fig. 5*A*) and holo-CI (Fig. 5*B*) of non-induced cells. These cells displayed a low steady-state ("leakage") expression of the tagged subunit due to small amounts of tetracycline in the culture medium. Using an identical analysis as for Fig. 2*D*, it was found that a maximum incorporation efficiency was reached for tNDUFA1, tNDUFS4, tNDUFS1, and tNDUFV2 (Fig. 5*D*; data points on the line of identity). In contrast, low efficiencies were reached for tNDUFA12 and tNDUFB6 (data points well below the line of identity).

Temporal Dynamics of Mitochondrial Import and CI Incorporation of AcGFP1-tagged CI Subunits—To determine the dynamics of subunit increase in mitoplasts and holo-CI, we investigated the amount of tagged subunit during the transition from low- to high-level expression. For this analysis, we used four key subunits (NDUFV1, NDUFS1, NDUFS3, and NDUFA2) that reached maximum incorporation into holo-CI within 24 h after induction and showed similar incorporation

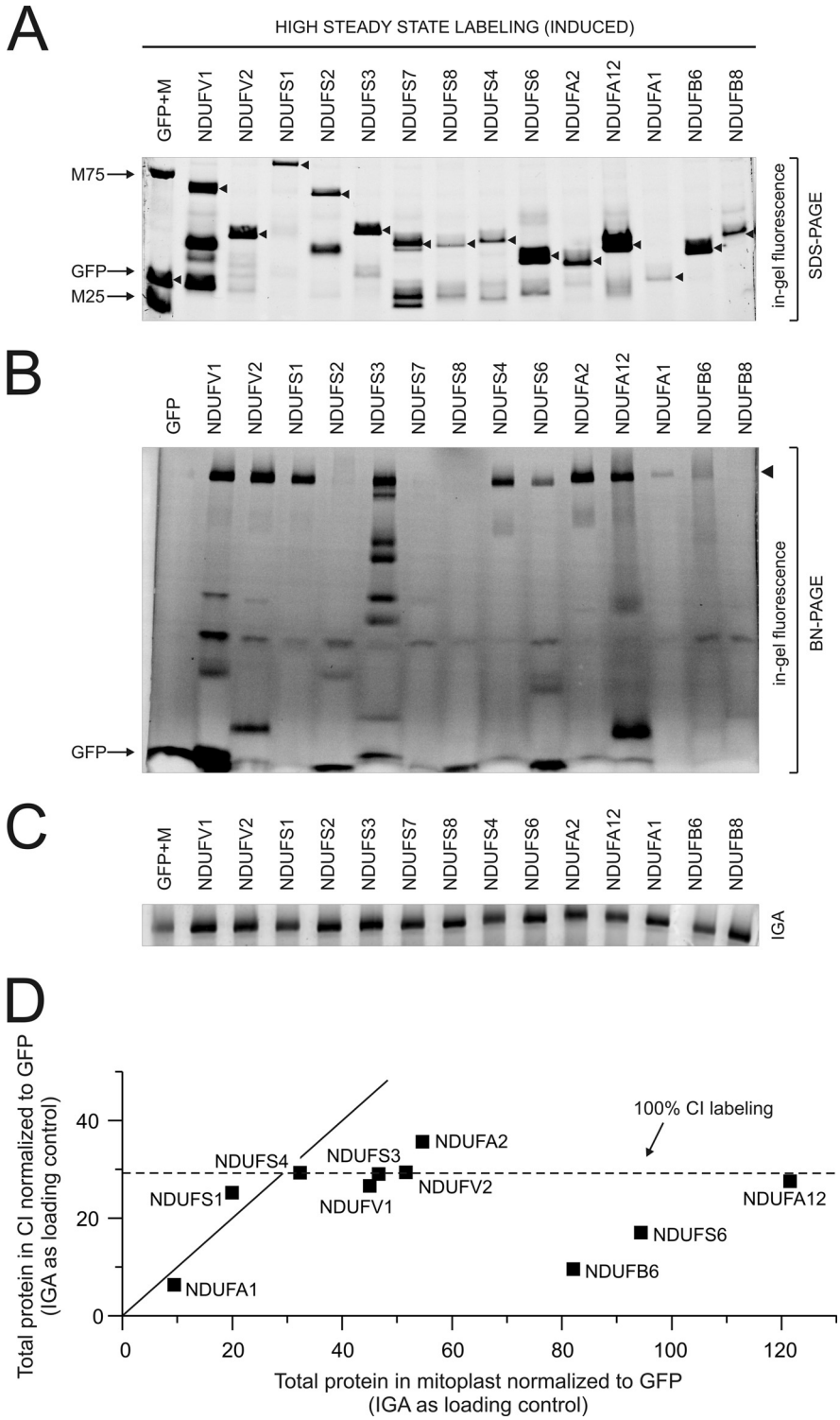

FIGURE 2. **Incorporation efficiency of AcGFP1-tagged CI subunits after induction with doxycycline.** *A*, cells were cultured in the presence of 1 μg/ml doxycycline for 24 h to obtain high steady-state expression. Identical protein amounts of isolated mitoplasts were subjected to SDS-PAGE, and gels were scanned for fluorescence. Bands of predicted MW are indicated with *filled arrowheads*. The *first lane* is from cells expressing matrix-targeted AcGFP1 (marked GFP) after addition of two MW marker proteins (marked M25 and M75) to the mitoplast sample. Lower MW bands reflect breakdown products (see also Ref. 20). *B*, identical protein amounts of the above mitoplast preparations were separated by BN-PAGE and scanned for fluorescence. The position of holo-CI is indicated with a *filled arrowhead*. *C*, the same gel as in *B* after staining for in-gel CI activity (IGA). Of note, compared with the gel in *B*, the *right* part of the gel in *C* is bent down because of the procedure for IGA measurement. *D*, incorporation efficiency plot of CI subunits. The fluorescence intensity of intact AcGFP1-tagged subunit on the SDS-PAGE fluorogram (*A*) was normalized to the corresponding IGA signal (*C*) and expressed as a percentage of the value obtained with intact matrix-targeted AcGFP1 (*x* axis). Similarly, the fluorescence intensity of holo-CI on the BN-PAGE fluorogram (*B*) was normalized to the corresponding IGA signal (*C*) and expressed as a percentage of the value obtained with intact matrix-targeted AcGFP1 (*y* axis). Thus, the *x* axis reflects the total amount of intact tagged subunit present in the mitoplasts, whereas the *y* axis reflects the amount of tagged subunit incorporated in holo-C1. The *solid line* (line of identity) indicates maximum incorporation efficiency, whereas the *dashed line* represents the maximum incorporation level.

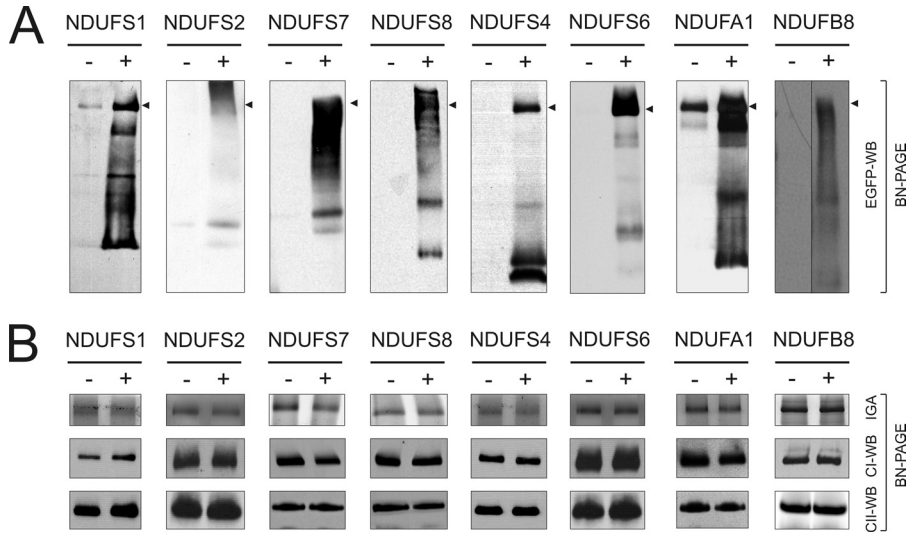

FIGURE 3. **Increased expression of tagged subunit has no effect on CI activity and/or assembly.** *A*, mitoplasts of non-induced (−) and induced (+) cells were subjected to BN-PAGE, blotted, and stained with an anti-EGFP antibody. *Filled arrowheads* indicate the position of holo-CI. Induction is apparent for all cell lines. *B*, induction has no effect on CI in-gel activity (*upper panels*), CI amount as detected with an anti-NDUFA9 antibody (*middle panel*), and CII amount as detected with an anti-SDHA antibody (*lower panel*). *WB*, Western blot.

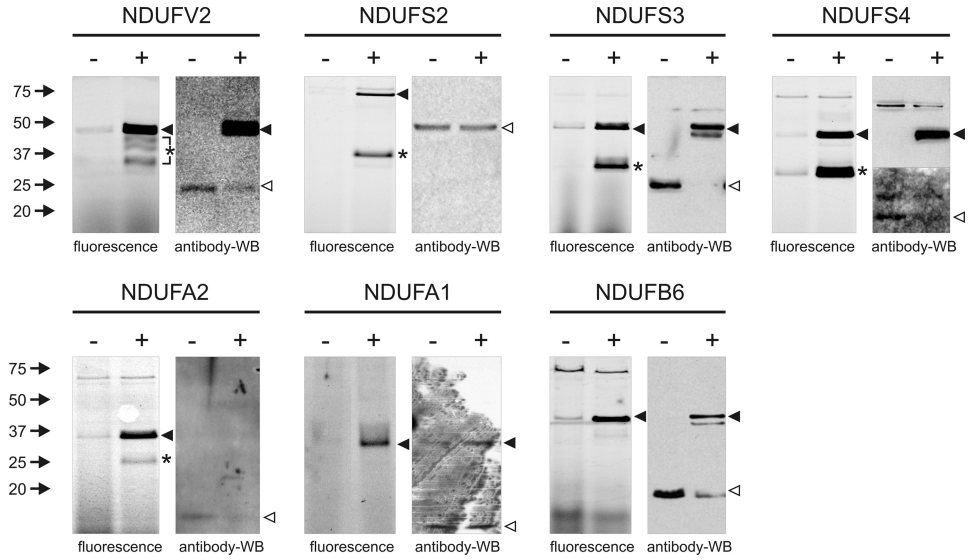

FIGURE 4. **Replacement of preexisting endogenous subunits by newly formed AcGFP1-tagged subunits in induced cells.** Mitoplasts of non-induced (−) and induced (+) cells were subjected to SDS-PAGE. Fluorograms confirm induction of AcGFP1-tagged subunits (panels labeled fluorescence). *Filled arrowheads* and *asterisks* indicate intact fusion protein and breakdown products, respectively (see also Ref. 20). Gels were blotted and probed with subunit-specific antibodies (panels labeled antibody-WB (Western blot)). In addition to endogenous subunit (*empty arrowheads*), often also its AcGFP1-tagged counterpart (*filled arrowheads*) was detected. Different exposure times were chosen for optimal visualization of endogenous and tagged NDUFS4.

efficiencies at low and high levels of steady-state expression (Fig. 6). Cells were harvested at various time points after induction and mitoplast proteins were separated by SDS- and BN-PAGE (for a typical example of such an experiment, see Fig. 1 of our previous study (4)). At each time point, we quantified the total amount of tagged subunit in the mitoplast or in holo-CI and normalized it to the corresponding IGA band. Values determined at 24 h were either set to the values in Fig. 2*D* (Fig. 6) or to 100% (Fig. 6; *insets*). The first normalization allows evaluation of the levels of tagged subunit in mitoplasts and holo-CI, whereas the second normalization enables better comparison of their import and incorporation kinetics.

For all tagged subunits, except tNDUFV1, mitoplast accumulation (*solid line*) and holo-CI incorporation (*dotted line*) reached a plateau within 24 h of induction. The time courses for mitoplast entry and holo-CI incorporation largely coincided for tNDUFS1 and tNDUFV1. This indicates that, once imported, incorporation of these subunits occurs rapidly. In contrast, for tNDUFS3 and tNDUFA2 CI incorporation clearly lagged behind their accumulation in the mitoplasts.

DISCUSSION

Data from previous studies with cells with a naturally or pharmacologically disturbed CI assembly have been interpreted to indicate that CI *de novo* synthesis occurs via several steps, in which subunits from different functional modules first form smaller assembly intermediates that are then combined to constitute the holoenzyme (3, 4, 6–9, 20). In addition, *in vitro*

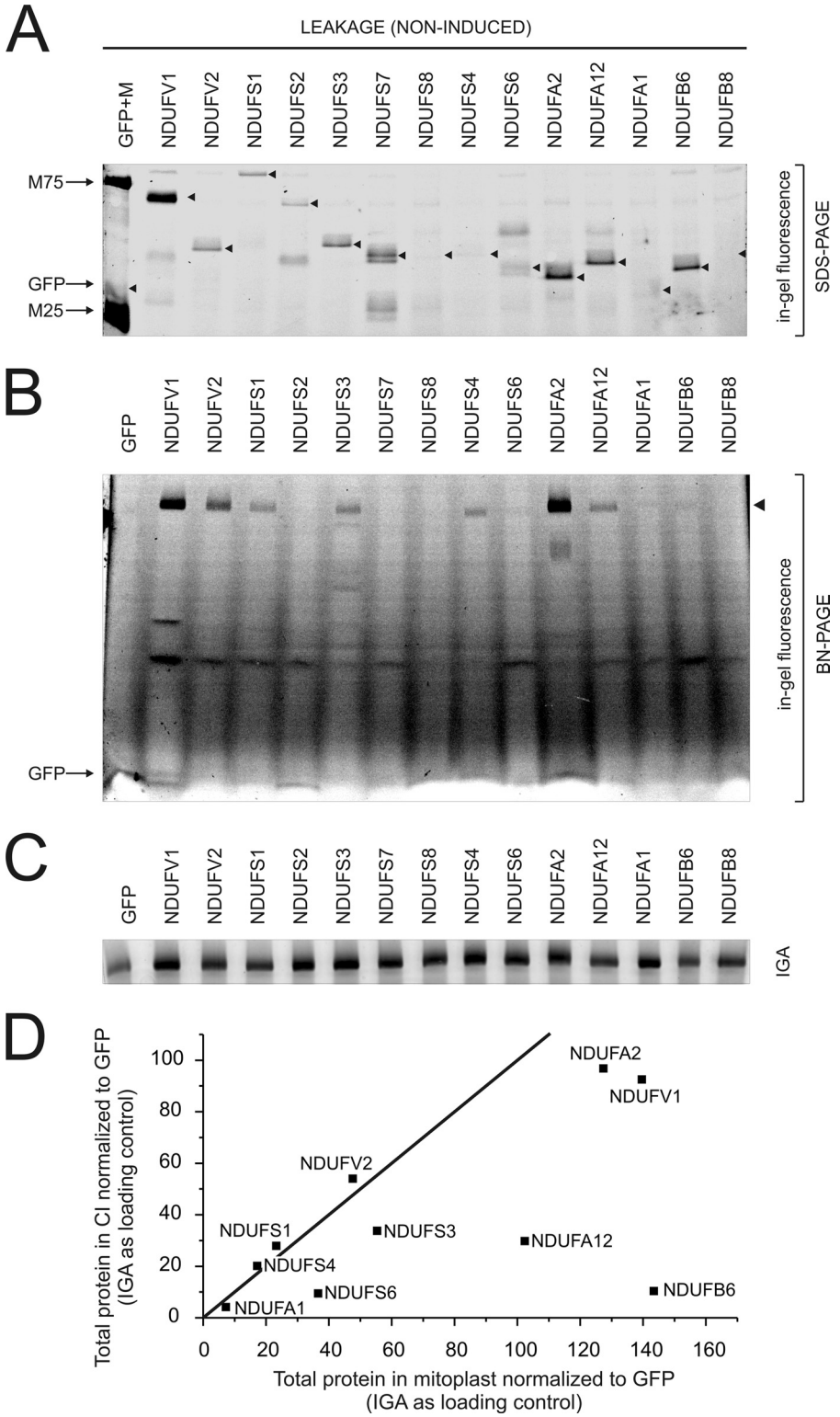

FIGURE 5. **Incorporation efficiency of AcGFP1-tagged CI subunits into holo-CI at low steady-state expression.** Cells were cultured in normal growth medium containing traces of tetracycline from FCS causing leakage expression. *A*, from each cell line, identical amounts of isolated mitoplasts were subjected to SDS-PAGE and scanned for fluorescence. Bands of predicted MW are indicated with *filled arrowheads*. The *first lane* is from mitoplasts of cells expressing matrix-targeted AcGFP1 (marked GFP) after addition of two MW marker proteins (marked M25 and M75). *B*, identical amounts of the same mitoplast preparations were separated by BN-PAGE and scanned for fluorescence. *Filled arrowheads* indicate the position of holo-CI. *C*, the same gel as in *B* after staining for in-gel CI activity. *D*, incorporation efficiency plot was constructed as described in the legend to Fig. 2*D*. The *x* axis shows the total amount of tagged subunit in the mitoplasts and the *y* axis depicts the amount in holo-CI. The *solid line* (line of identity) indicates maximum incorporation efficiency.

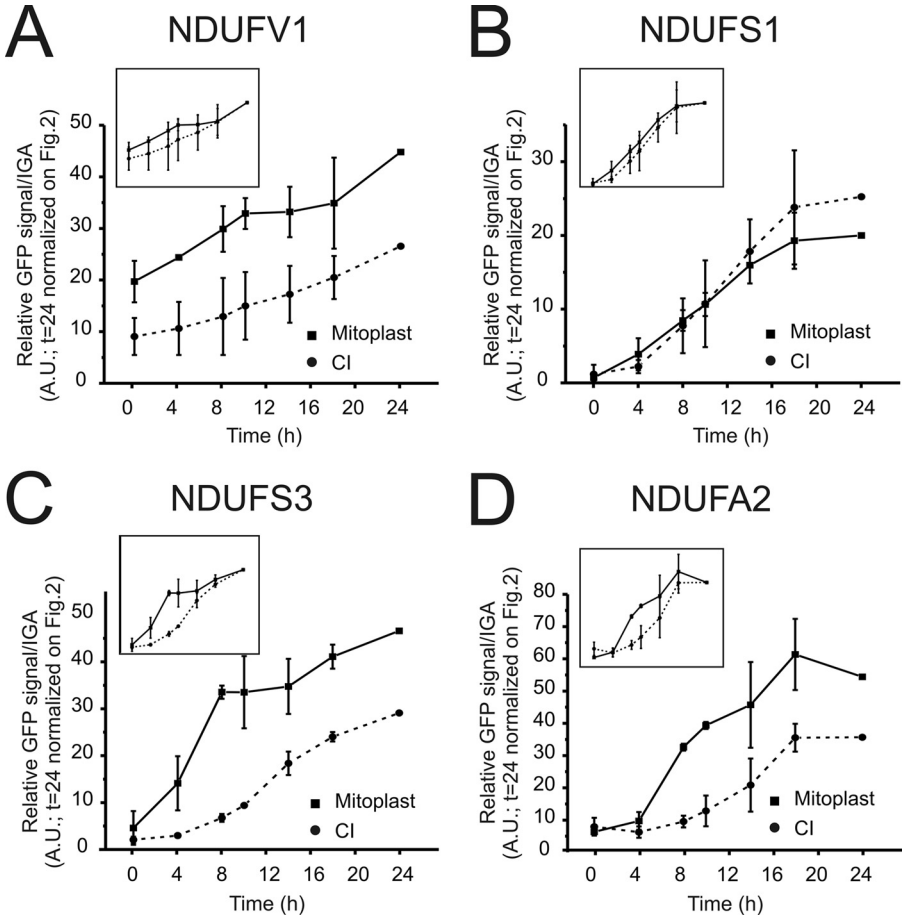

FIGURE 6. **Kinetics of mitochondrial import and CI incorporation of AcGFP1-tagged CI subunits.** Mitoplasts were isolated at different time points after induction with 1 μg/ml doxycycline in two independent experiments (original gels not shown). (For a typical example, see Fig. 1 of our previous study (4).) SDS- and BN-PAGE gels were either blotted and probed with an anti-EGFP antibody (experiment 1) or scanned for fluorescence (experiment 2). Similar results were obtained in both experiments demonstrating the interchangeability of the two GFP detection techniques for this analysis. Subunit levels in mitoplasts and in holo-CI were quantified for each time point and normalized to the corresponding IGA signal. For each subunit, the values at 24 h were set at either the corresponding values in Fig. 2*D* or at 100% (*inset*). *Error bars* indicate the variation observed in the two individual experiments. *A.U.*, arbitrary units.

labeling studies provided evidence for the existence of a direct exchange of some CI subunits into CI without the interference of assembly intermediates (8). It was proposed that this mechanism functions to "fix" oxidatively damaged subunits in an efficient manner. However, the relative importance of these two incorporation modes under physiological conditions was never investigated. In this study, we made use of cell lines that conditionally express AcGFP1-tagged CI subunits to investigate the assembly characteristics of different subunits during CI maintenance in a quantitative manner. To this end, we determined the ratio between the amount of tagged subunit present in holo-CI and the total amount of tagged subunit present in mitoplasts at low and high level of steady-state expression, and during the transition between these two states. Of the 14 AcGFP1-tagged CI subunits that were investigated, four (tNDUFS2, tNDUFS7, tNDUFS8, and tNDUFB8) were not or insufficiently incorporated into holo-CI, precluding their further analysis in this study. Importantly, low *versus* high steady-state expression of the other tagged subunits did not affect CI protein amount and/or activity. This means that none of these subunits is rate-limiting in CI assembly and that subunit-tagging does not detrimentally affect assembly and/or activity of holo-CI.

After 24 h of high level induction, we observed that seven of the tagged subunits displayed a similar fluorescence intensity at the position of holo-CI on a BN-PAGE gel. These subunits included NDUFS1, NDUFV1, and NDUFV2 of the dehydrogenase module, NDUFS3 of the hydrogenase module, and the accessory peripheral arm subunits NDUFS4, NDUFA2, and NDUFA12 of unknown function. Analysis of endogenous subunit levels showed that tNDUFS3 completely outcompeted its endogenous counterpart, indicating that this fluorescence intensity represents the maximum possible level of CI labeling. This demonstrates for the first time that NDUFV1, NDUFV2, NDUFS1, NDUFS3, NDUFS4, NDUFA2, and NDUFA12 are present in a similar stoichiometric amount in mammalian holo-CI. Previous studies have shown that each individual subunit occurs once per CI molecule in the bacterium *Thermus thermophilus* (1, 24), which makes it likely that the same holds true for the much larger mammalian CI. Our data confirm this widely accepted, yet unproven assumption for at least these seven subunits.

Previous studies, which first induced complete depletion of CI by transient inhibition of mitochondrial translation, report CI restoration times of 2–4 days (3, 12–14). The present finding that endogenous NDUFV1, NDUFV2, NDUFS1, NDUFS3,

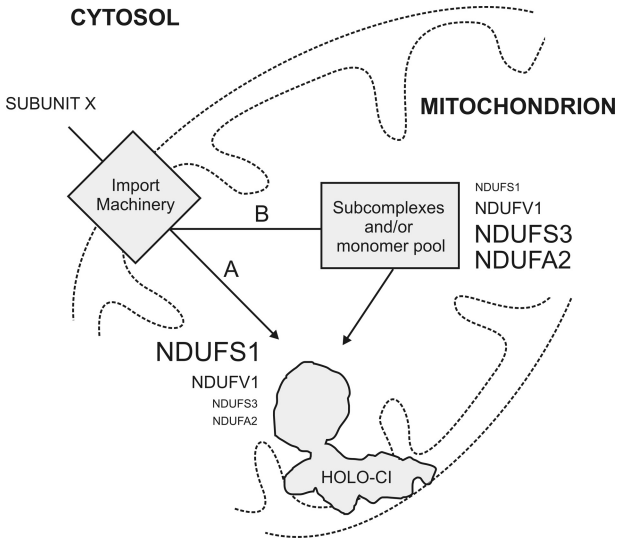

FIGURE 7. **Proportional use of direct and indirect (delayed) subunit incorporation during CI maintenance.** Incorporation of some subunits into CI occurs immediately after import into the mitochondrion (route *A*). Other subunits are initially stored in monomer pools and/or assembled into subcomplexes, prior to incorporation into holo-CI (route *B*). This results in a delay in appearance in holo-CI after import in the mitochondrial matrix. The relative proportion of each incorporation mode (route) for NDUFV1, NDUFS1, NDUFS3, and NDUFA2 is reflected by *font size*.

NDUFS4, NDUFA2, and NDUFA12 were fully replaced by their tagged counterparts in holo-CI after 24 h of induction, indicates that the turnover of these subunits during CI maintenance occurs within this time frame and thus is faster than expected. Indeed, steady-state labeling of holo-CI was reached within 24 h during the transition from low- to high-level expression of tNDUFS1, tNDUFS3, and tNDUFA2. Noticeably, the increase in the amount of tagged subunit in the mitoplasts ceased at the same time that all endogenous NDUFS1, NDUFS3, or NDUFA2 was replaced by its tagged counterpart, indicating that the mitoplast levels of these subunits are tightly regulated. The latter is in concordance with our observation that the holo-CI/mitoplast ratios of the other subunits also remained virtually unchanged under high and low expression levels. The exception was tNDUFV2, which showed maximal incorporation efficiency under leakage conditions but accumulation of monomeric subunit on native gel upon induction.

The ability to determine the fraction of total mitoplast fusion protein present in holo-CI revealed that some subunits (tNDUFS1, tNDUFS4, and tNDUFA1) showed maximal incorporation efficiencies at low and high levels of steady-state expression. This strongly suggests that these subunits are directly built in into holo-CI upon import and, in quantitative terms, are not present in assembly intermediates (for schematic representation of our findings, we refer to Fig. 7). In line with this finding, the curves displaying the amount of tNDUFS1 in mitoplasts and holo-CI during the transition from low to high expression levels overlapped. In conclusion, NDUFS1 seems to use predominantly a direct incorporation mode (Fig. 7), compatible with the exchange model (8). In contrast, other subunits had suboptimal incorporation efficiencies. For two subunits with intermediate incorporation efficiencies (tNDUFS3 and tNDUFA2), labeling of mitoplasts clearly preceded that of holo-CI during time induction experiments. In other words, these subunits are primarily incorporated into subassemblies and/or are present as monomers before they are assembled into CI (Fig. 7). Also, tNDUFV1 was found to be present in CI subassemblies. However, in contrast to tNDUFS3 and tNDUFA2, its labeling kinetics of mitoplasts and holo-CI were identical. This strongly suggests that tNDUFV1 makes use of both incorporation modes, in which a certain amount of tNDUFV1 can be directly incorporated into CI upon import, whereas the remainder assembles into smaller (sub)complexes and/or is stored in a NDUFV1 monomer pool (Fig. 7). Newly synthesized subunits were found to assemble at different rates into holo-CI in *N. crassa*, and it was concluded that this was due to differences in pool size (10). However, our data support the alternative explanation that the different assembly rates reflect the involvement of assembly intermediates.

Obviously, CI biogenesis is much more intricate than represented by the current CI assembly models. For instance, the previous paragraph concluded that two subunits of the dehydrogenase module (tNDUFV1 and tNDUFS1) have distinct incorporation patterns. Several qualitative studies proposed that these two subunits assemble together with other subunits from the same module (3, 4, 25), whereas an *in vitro* import study reported that NDUFS1 assembled with subunits of the hydrogenase module (8). Both models are very plausible, since NDUFS1 is a functional constituent of both the dehydrogenase and hydrogenase module (24, 26, 27). It is tempting to speculate that NDUFS1 is capable to assemble via both modules, depending on cell type and/or metabolic state. Fig. 1*D* shows that tNDUFV1 and tNDUFS1 display similar subcomplexes as tNDUFV2 on a BN-PAGE gel probed with an anti-EGFP antibody. NDUFV2 is also a core subunit of the dehydrogenase module (28), suggesting that in our setting these three subunits assemble into dehydrogenase subcomplexes. However, we discussed already that tNDUFS1, in contrast to tNDUFV1 and tNDUFV2, was virtually absent in smaller subassemblies after 24 h of induction. The fact that CI labeling for these three subunits was equal, whereas their incorporation levels in subcomplexes differed, makes it unlikely that these subassemblies represent isolation artifacts or breakdown products. Therefore, we propose that these subunits exchange at different rates with already incorporated subunits in subcomplexes during CI homeostasis. This resembles the proposed mechanism for subunit exchange in holo-CI (8).

Recently, it is suggested that assembly intermediates of CI might serve as scaffold for the assembly of other respiratory chain complexes during the formation of respirasomes (14). In line with our findings, the incorporation kinetics of nuclear encoded CI subunits into so called supercomplexes after inhibition of mitochondrial translation occurred for some subunits (NDUFS2 and NDUFA9) faster that for others (NDUFS4 and NDUFV1) (14). Our data further suggest that the NDUFV1 pool size is relatively large and has a fast turnover, compatible with the abundance of tNDUFV1 breakdown products. This might be explained by the presence of the NADH binding site, flavin mononucleotide and N3 iron-sulfur cluster (24, 29, 30), which could render this subunit more vulnerable to oxidants than other dehydrogenase subunits.

In conclusion, our approach of tagging CI subunits with AcGFP1 provided several new quantitative opportunities to study CI assembly in terms of stoichiometry, incorporation efficiency and temporal assembly dynamics. Subunits of CI are under continuous threat of oxidative damage because CI function is inextricably linked with the production of reactive oxygen species. It is, therefore, important to have detailed knowledge of the mechanisms involved in maintaining the integrity of the complex. This knowledge will contribute to a better understanding of pathologies related to CI dysfunction (31, 32).

REFERENCES

1. Efremov, R. G., Baradaran, R., and Sazanov, L. A. (2010) The architecture of respiratory complex I. *Nature* **465,** 441–445
2. Balsa, E., Marco, R., Perales-Clemente, E., Szklarczyk, R., Calvo, E., Landázuri, M. O., and Enríquez, J. A. (2012) NDUFA4 is a subunit of complex IV of the mammalian electron transport chain. *Cell Metab.* **16,** 378–386
3. Ugalde, C., Vogel, R., Huijbens, R., Van Den Heuvel, B., Smeitink, J., and Nijtmans, L. (2004) Human mitochondrial complex I assembles through the combination of evolutionary conserved modules: a framework to interpret complex I deficiencies. *Hum. Mol. Genet.* **13,** 2461–2472
4. Vogel, R. O., Dieteren, C. E., van den Heuvel, L. P., Willems, P. H., Smeitink, J. A., Koopman, W. J., and Nijtmans, L. G. (2007) Identification of mitochondrial complex I assembly intermediates by tracing tagged NDUFS3 demonstrates the entry point of mitochondrial subunits. *J. Biol. Chem.* **282,** 7582–7590
5. Koopman, W. J., Nijtmans, L. G., Dieteren, C. E., Roestenberg, P., Valsecchi, F., Smeitink, J. A., and Willems, P. H. (2010) Mammalian mitochondrial complex I: biogenesis, regulation, and reactive oxygen species generation. *Antioxid. Redox. Signal.* **12,** 1431–1470
6. Vogel, R. O., Smeitink, J. A., and Nijtmans, L. G. (2007) Human mitochondrial complex I assembly: a dynamic and versatile process. *Biochim. Biophys. Acta* **1767,** 1215–1227
7. Antonicka, H., Ogilvie, I., Taivassalo, T., Anitori, R. P., Haller, R. G., Vissing, J., Kennaway, N. G., and Shoubridge, E. A. (2003) Identification and characterization of a common set of complex I assembly intermediates in mitochondria from patients with complex I deficiency. *J. Biol. Chem.* **278,** 43081–43088
8. Lazarou, M., McKenzie, M., Ohtake, A., Thorburn, D. R., and Ryan, M. T. (2007) Analysis of the assembly profiles for mitochondrial- and nuclear-DNA-encoded subunits into complex I. *Mol. Cell. Biol.* **27,** 4228–4237
9. Perales-Clemente, E., Fernández-Vizarra, E., Acín-Pérez, R., Movilla, N., Bayona-Bafaluy, M. P., Moreno-Loshuertos, R., Pérez-Martos, A., Fernández-Silva, P., and Enríquez, J. A. (2010) Five entry points of the mitochondrially encoded subunits in mammalian complex I assembly. *Mol. Cell. Biol.* **30,** 3038–3047
10. Videira, A., and Werner, S. (1989) Assembly kinetics and identification of precursor proteins of complex I from *Neurospora crassa*. *Eur. J. Biochem.* **181,** 493–502
11. Hall, R. E., and Hare, J. F. (1990) Respiratory chain-linked NADH dehydrogenase. Mechanisms of assembly. *J. Biol. Chem.* **265,** 16484–16490
12. Pello, R., Martín, M. A., Carelli, V., Nijtmans, L. G., Achilli, A., Pala, M., Torroni, A., Gómez-Durán, A., Ruiz-Pesini, E., Martinuzzi, A., Smeitink, J. A., Arenas, J., and Ugalde, C. (2008) Mitochondrial DNA background modulates the assembly kinetics of OXPHOS complexes in a cellular model of mitochondrial disease. *Hum. Mol. Genet.* **17,** 4001–4011
13. Yadava, N., Houchens, T., Potluri, P., and Scheffler, I. E. (2004) Development and characterization of a conditional mitochondrial complex I assembly system. *J. Biol. Chem.* **279,** 12406–12413
14. Moreno-Lastres, D., Fontanesi, F., García-Consuegra, I., Martín, M. A., Arenas, J., Barrientos, A., and Ugalde, C. (2012) Mitochondrial complex I plays an essential role in human respirasome assembly. *Cell Metab.* **15,** 324–335
15. Potluri, P., Yadava, N., and Scheffler, I. E. (2004) The role of the ESSS protein in the assembly of a functional and stable mammalian mitochondrial complex I (NADH-ubiquinone oxidoreductase). *Eur. J. Biochem.* **271,** 3265–3273
16. Triepels, R. H., Hanson, B. J., van den Heuvel, L. P., Sundell, L., Marusich, M. F., Smeitink, J. A., and Capaldi, R. A. (2001) Human complex I defects can be resolved by monoclonal antibody analysis into distinct subunit assembly patterns. *J. Biol. Chem.* **276,** 8892–8897
17. Bourges, I., Ramus, C., Mousson de Camaret, B., Beugnot, R., Remacle, C., Cardol, P., Hofhaus, G., and Issartel, J. P. (2004) Structural organization of mitochondrial human complex I: role of the ND4 and ND5 mitochondria-encoded subunits and interaction with prohibitin. *Biochem. J.* **383,** 491–499
18. Dieteren, C. E., Willems, P. H., Swarts, H. G., Fransen, J., Smeitink, J. A., Koopman, W. J., and Nijtmans, L. G. (2011) Defective mitochondrial translation differently affects the live cell dynamics of complex I subunits. *Biochim. Biophys. Acta* **1807,** 1624–1633
19. Dieteren, C. E., Koopman, W. J., and Nijtmans, L. G. (2009) Tracing human mitochondrial complex I assembly by use of GFP-tagged subunits. *Methods Enzymol.* **456,** 133–151
20. Dieteren, C. E., Willems, P. H., Vogel, R. O., Swarts, H. G., Fransen, J., Roepman, R., Crienen, G., Smeitink, J. A., Nijtmans, L. G., and Koopman, W. J. (2008) Subunits of mitochondrial complex I exist as part of matrix- and membrane-associated subcomplexes in living cells. *J. Biol. Chem.* **283,** 34753–34761
21. Dieteren, C. E., Gielen, S. C., Nijtmans, L. G., Smeitink, J. A., Swarts, H. G., Brock, R., Willems, P. H., and Koopman, W. J. (2011) Solute diffusion is hindered in the mitochondrial matrix. *Proc. Natl. Acad. Sci. U.S.A.* **108,** 8657–8662
22. Zuo, D., Mohr, S. E., Hu, Y., Taycher, E., Rolfs, A., Kramer, J., Williamson, J., and LaBaer, J. (2007) PlasmID: a centralized repository for plasmid clone information and distribution. *Nucleic Acids Res.* **35,** D680–684
23. Calvaruso, M. A., Smeitink, J., and Nijtmans, L. (2008) Electrophoresis techniques to investigate defects in oxidative phosphorylation. *Methods* **46,** 281–287
24. Sazanov, L. A., and Hinchliffe, P. (2006) Structure of the hydrophilic domain of respiratory complex I from *Thermus thermophilus*. *Science* **311,** 1430–1436
25. Schneider, D., Pohl, T., Walter, J., Dörner, K., Kohlstädt, M., Berger, A., Spehr, V., and Friedrich, T. (2008) Assembly of the *Escherichia coli* NADH:ubiquinone oxidoreductase (complex I). *Biochim. Biophys. Acta* **1777,** 735–739
26. Pilkington, S. J., Skehel, J. M., Gennis, R. B., and Walker, J. E. (1991) Relationship between mitochondrial NADH-ubiquinone reductase and a bacterial NAD-reducing hydrogenase. *Biochemistry* **30,** 2166–2175
27. Yamaguchi, M., and Hatefi, Y. (1993) Mitochondrial NADH:ubiquinone oxidoreductase (complex I): proximity of the subunits of the flavoprotein and the iron-sulfur protein subcomplexes. *Biochemistry* **32,** 1935–1939
28. Friedrich, T., and Weiss, H. (1997) Modular evolution of the respiratory NADH:ubiquinone oxidoreductase and the origin of its modules. *J. Theor. Biol.* **187,** 529–540
29. Finel, M., Skehel, J. M., Albracht, S. P., Fearnley, I. M., and Walker, J. E. (1992) Resolution of NADH:ubiquinone oxidoreductase from bovine heart mitochondria into two subcomplexes, one of which contains the redox centers of the enzyme. *Biochemistry* **31,** 11425–11434
30. Hirst, J., Carroll, J., Fearnley, I. M., Shannon, R. J., and Walker, J. E. (2003) The nuclear encoded subunits of complex I from bovine heart mitochondria. *Biochim. Biophys. Acta* **1604,** 135–150
31. Smeitink, J., van den Heuvel, L., and DiMauro, S. (2001) The genetics and pathology of oxidative phosphorylation. *Nat. Rev. Genet.* **2,** 342–352
32. Janssen, R. J., Nijtmans, L. G., van den Heuvel, L. P., and Smeitink, J. A. (2006) Mitochondrial complex I: structure, function, and pathology. *J. Inherit. Metab. Dis.* **29,** 499–515